Pergamon

Int. J. Heat Mass Transfer. Vol. 39, No. 15, pp. 3101–3115, 1996

0017-9310/96 $15.00 + 0.00

PII: S0017-9310(96)00005-1

Numerical prediction of laminar flow and forced convective heat transfer in a helical square duct with a finite pitch

C. JONAS BOLINDER and BENGT SUNDÉN†

Division of Heat Transfer, Lund Institute of Technology, Box 118, 221 00 Lund, Sweden

(*Received* 21 *November* 1994 *and in final form* 19 *December* 1995)

Abstract—Fully developed laminar forced convective heat transfer in helical square ducts is studied numerically using a finite-volume method. The *H*1 thermal boundary condition is applied. Dean numbers up to 510 and Prandtl numbers between 0.005 and 500 are considered. Correlations for the mean Nusselt number are proposed. For a toroidally curved duct, two solution branches with a two-vortex secondary flow and one branch with a four-vortex flow are detected. The four-vortex solutions give, for high *Pr*, mean Nusselt numbers up to twice those of the two-vortex solutions. For ducts of small pitch or torsion, the flow and heat transfer characteristics are similar to those of a toroidally curved duct with the same dimensionless curvature ε. Copyright © 1996 Elsevier Science Ltd.

INTRODUCTION

A characteristic feature of flow in curved ducts is the so-called secondary flow, which is set up due to the centrifugal force. The secondary flow is the projection of the fluid velocity onto the cross-plane of the duct. For a toroidally curved duct, for example, the secondary flow often consists of two symmetric counter-rotating cells. The secondary flow increases the mean heat and mass transfer rates, a phenomenon utilized in industrial applications, as for example in heat transfer equipment, chemical processes and medical equipment. The increased transfer rates of curved ducts, compared to those of straight ducts, are most prominent for laminar flow. For turbulent flow, according to Shah and Joshi [1], curved ducts offer no other significant advantage than space saving.

Previous works on fluid flow and convective heat transfer in curved ducts are reviewed in refs. [1–3]. Mostly toroidally curved ducts of circular cross-section have been considered in the past. Ducts of rectangular cross-section have not been greatly investigated, especially with respect to convective heat transfer. Also helically coiled ducts with a finite pitch have been studied quite sparsely. The latter circumstance may be due to the increased mathematical complexity associated with the finite pitch. Often the helical geometry is modelled by providing the centreline of the duct with a finite torsion, apart from the finite curvature characteristic of any curved duct. The torsion gives rise to the pitch, and it also makes the associated coordinate system nonorthogonal. For a nonorthogonal coordinate system, the choice of velocity components is not obvious. The components obtained from an expansion of the velocity vector in the so-called natural basis are called contravariant. The base vectors of the natural basis are tangents to the coordinate curves. Thus, for nonorthogonal coordinate system, the natural basis is nonorthogonal, and it is inconvenient to use. It is preferable to use a physical, i.e. an orthonormal, basis for the velocity, since then the (physical) velocity components are obtained as the projections of the velocity vector on the respective physical base vectors. The recommended choice of physical basis is the tangent **t**, normal **n** and binormal **b** of the centre-line of the duct. Among the previous authors on helical duct flows, both physical and contravariant components have been employed, and different conclusions about the effect of torsion on the flow have been put forward, see Bolinder [4, 5] for a review. The convenience of using physical components is also demonstrated in the experimental investigation by Bolinder and Sundén [6].

Laminar forced convection in toroidally curved ducts of rectangular cross-section has been studied for example by Cheng and Akiyama [7] and by Mori *et al.* [8]. They considered fully developed conditions and applied the *H*1 thermal boundary condition, i.e. constant wall heat flux in the axial direction and uniform wall temperature peripherally. Mori *et al.* also carried out experiments. Cheng *et al.* [9] studied thermally developing flow with the *T* and *H*2 boundary conditions, i.e. uniform wall temperature and uniform wall heat flux, respectively. The asymptotic Nusselt number was found to be similar for the two boundary conditions, and a single correlation was given, presumed to be valid for both conditions. Komiyama *et al.* [10] investigated ducts with varying aspect ratio,

† Author to whom correspondence should be addressed.

NOMENCLATURE

a half width of duct
A_w (wetted) wall area of duct, equation (17)
b half height of duct
$\mathbf{b}$ binormal of centre-line $\mathbf{t} \times \mathbf{n}$
C_p specific heat
d_h hydraulic diameter, $4ab/(a+b)$
De Dean number, $Re\sqrt{\kappa d_h}$
$\mathbf{e}_r$, $\mathbf{e}_\theta$, $\mathbf{e}_z$ unit base vectors of cylindrical coordinate system, see Fig. 1
E efficiency, equation (29)
f friction factor, $-(\partial p/\partial s)d_h/(2\rho\bar{w}^2)$
h heat transfer coefficient, $q_N/(T_w - T_b)$
k thermal conductivity
$2\pi K$ pitch of helical duct, $2\pi\tau/(\kappa^2+\tau^2)$
L_1, L_2, L_3, L_8 limit points, one-sided bifurcation points
M $1-\kappa x$
$\mathbf{n}$ normal of centre-line, $\mathbf{r}_c''/\kappa$
$\mathbf{N}$ inward-pointing unit normal, equation (16)
Nu Nusselt number, hd_h/k
p generalized pressure, including effect of gravity
Pr Prandtl number, $C_p\rho\nu/k$
q_N inward heat flux normal to duct wall [W m^{-2}], equation (14)
$\mathbf{r}$ position vector, equation (7)
$\mathbf{r}_c$ position vector of centre-line, equation (1)
R radius of helical duct, $\kappa/(\kappa^2+\tau^2)$
Re Reynolds number, $\bar{w}d_h/\nu$
s arc length of centre-line, streamwise coordinate
S_1, S_3, S_5 solution branches
t time
$\mathbf{t}$ tangent of centre-line, $\mathbf{r}_c'$
T temperature
T_0 $T-\gamma_s$
T_b bulk mean temperature, equation (20)
u, v secondary flow components, $\mathbf{v}\cdot\mathbf{n}$ and $\mathbf{v}\cdot\mathbf{b}$, respectively
U, V dimensionless secondary flow components, $(u, v)d_h/\nu$
$\mathbf{v}$ velocity vector
w axial flow component, $\mathbf{v}\cdot\mathbf{t}$
$\bar{w}$ mean axial flow
x, y coordinates along $\mathbf{n}$ and $\mathbf{b}$, respectively.

Greek symbols

α slope of centre-line, equation (4)
γ axial temperature gradient, $\partial T/\partial s$
ε dimensionless curvature, κd_h
η dimensionless torsion, τd_h
θ dimensionless temperature, $(T_w - T_0)/\gamma d_h$
ϑ angle along centre-line, $s/\sqrt{R^2+K^2}$
κ curvature of centre-line, $R/(R^2+K^2)$
ν kinematic viscosity
ρ density
τ torsion of centre-line, $K/(R^2+K^2)$.

Subscripts

m peripheral mean value
s value for straight duct
w value at duct wall.

Superscript

′ derivative with respect to s.

utilizing the $H1$ boundary condition. More recently Hwang and Chao [11] considered fully developed conditions with the T boundary condition, but without neglecting the axial conduction term in the energy equation.

The effect of a finite pitch on laminar forced convective heat transfer has been studied in a few recent papers. Yang *et al.* [12] and Liu and Masliyah [13] considered ducts of circular cross-section. Curiously enough, the asymptotic temperature profiles of Liu and Masliyah (their Fig. 10) differ significantly from those of Yang *et al.* (their Fig. 2), despite the fact that similar conditions prevail. Yang *et al.* predict a 'rotated' profile for $Pr = 1$, and a strongly skew profile for $Pr = 10$. Liu and Masliyah [13] predict a much weaker effect of a relatively small torsion. Considering the results of the present investigation, the predictions by Liu and Masliyah seem more reliable. Eason *et al.* [14] analysed simultaneously developing flow and heat transfer in square helical ducts applying the T boundary condition. They considered a duct with a relatively small pitch and with varying curvature. The governing equations were solved using a commercial finite element code. Thus, they were not able to take advantage of the exact problem formulation available by describing the geometry in terms of the curvature and the torsion of the centre-line of the duct (see the next section). No specific information on the method of generating the duct geometry was given.

A few studies on laminar forced convective heat transfer in straight twisted rectangular ducts have been carried out, e.g. by Masliyah and Nandakumar [15] and Nandakumar and Masliyah [16], who applied the T boundary condition. A straight twisted duct is characterized by the centre-line having a zero curvature and a nonzero torsion, and is thus related to the helical duct. It was found in refs. [15, 16] that the mean Nusselt number for a straight twisted square

duct always is lower than that for a straight untwisted duct. For a rectangular twisted duct with an aspect ratio differing from one, a slight enhancement of the Nusselt number was obtained for certain flow conditions.

In this investigation, fully developed laminar forced convective heat transfer in helical square ducts is analysed numerically using the finite-volume method. The $H1$ thermal boundary condition is applied, which may be realized experimentally for example in electrically heated ducts with highly conductive walls. The study is based on the flow field analysis presented in Bolinder [4, 5], and it thus features the pure effect of torsion on the heat transfer characteristics keeping the curvature fixed. In addition to the mean Nusselt number, the local peripheral variation of the Nusselt number is provided for a few cases. Prandtl numbers between 0.005 and 500 are considered.

GOVERNING EQUATIONS

The position vector of the centre-line of a helical duct may be written

$$\mathbf{r}_{c(s)} = R\mathbf{e}_r(s) + K\vartheta(s)\mathbf{e}_z, \quad \text{where } \vartheta(s) = s/\sqrt{R^2+K^2}. \tag{1}$$

The parameter s, which is the arc length of the centre-line, is used as a coordinate along the duct. ϑ is a polar angle, R is the radius of the cylinder to which the centre-line is coiled, and $2\pi K$ is the so-called pitch, see Fig. 1. $\mathbf{e}_r$, $\mathbf{e}_\theta$ and $\mathbf{e}_z$ are unit base vectors of the cylindrical coordinate system indicated in Fig. 1. The tangent $\mathbf{t}$, normal $\mathbf{n}$ and binormal $\mathbf{b}$ of $\mathbf{r}_c$ are defined by

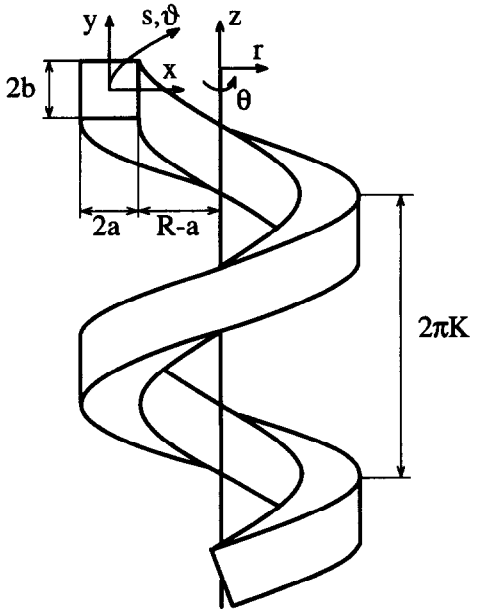

Fig. 1. Helical square duct.

$$\mathbf{t} = \mathbf{r}_c', \quad \mathbf{n} = \frac{1}{\kappa}\mathbf{r}_c'', \quad \mathbf{b} = \mathbf{t}\times\mathbf{n}, \tag{2}$$

where $'$ denotes a derivative with respect to s. Note that $\mathbf{t}$, $\mathbf{n}$ and $\mathbf{b}$ are orthonormal. For the helical centre-line described by equation (1), one obtains

$$\left.\begin{aligned} \mathbf{t}(s) &= \cos\alpha\mathbf{e}_\theta(s) + \sin\alpha\mathbf{e}_z, \\ \mathbf{n}(s) &= -\mathbf{e}_r(s), \\ \mathbf{b}(s) &= -\sin\alpha\mathbf{e}_\theta(s) + \cos\alpha\mathbf{e}_z \end{aligned}\right\}. \tag{3}$$

α is the slope of the centre-line relative to the plane z = constant. One finds that

$$\cos\alpha = \frac{R}{\sqrt{R^2+K^2}}, \sin\alpha = \frac{K}{\sqrt{R^2+K^2}}. \tag{4}$$

The curvature κ and the torsion τ of $\mathbf{r}_c$ are defined by

$$\kappa = |\mathbf{r}_c''|, \quad \tau = \mathbf{n}'\cdot\mathbf{b}. \tag{5}$$

Equation (1) gives

$$\kappa = \frac{R}{R^2+K^2}, \quad \tau = \frac{K}{R^2+K^2}. \tag{6}$$

It is illustrative to evaluate equations (3), (4) and (6) for the special cases of a toroidal duct ($K = \tau = 0$) and a straight twisted duct ($R = \kappa = 0$). Let x be a coordinate along the normal $\mathbf{n}$ and y a coordinate along the binormal $\mathbf{b}$, according to Fig. 1. Then the position vector of any point in the duct may be written

$$\mathbf{r}(s,x,y) = \mathbf{r}_c(s) + x\mathbf{n}(s) + y\mathbf{b}(s). \tag{7}$$

The so-called natural base vectors of the coordinate system (s,x,y) are obtained as the partial derivatives of $\mathbf{r}$ with respect to the coordinates, they are thus tangents to the coordinate curves. One finds that the natural base vectors are nonorthogonal for points off the centre-line, except for a toroidal duct (with $\tau = 0$). By expanding the velocity vector in the natural basis, the so-called contravariant velocity components are obtained. However, as discussed in the introduction, if the natural basis is nonorthogonal it is more appropriate to expand the velocity in the physical basis $(\mathbf{t},\mathbf{n},\mathbf{b})$. Accordingly one has

$$\mathbf{v} = w\mathbf{t} + u\mathbf{n} + v\mathbf{b}, \tag{8}$$

where w is the axial flow, and u and v constitute the secondary flow.

The continuity equation and the Navier–Stokes equations, expressed in terms of the coordinates s, x and y and the physical velocity components w, u and v, and assuming an incompressible and fully developed flow, are given by

$$\frac{\partial}{\partial x}(Mu + \tau yw) + \frac{\partial}{\partial y}(Mv - \tau xw) = 0, \tag{9}$$

$$\frac{\partial w}{\partial t}+\left(u+\frac{\tau y}{M}w\right)\frac{\partial w}{\partial x}+\left(v-\frac{\tau x}{M}w\right)\frac{\partial w}{\partial y}-\frac{\kappa}{M}wu$$
$$=-\frac{1}{\rho M}\left(\frac{\partial p}{\partial s}+\tau y\frac{\partial p}{\partial x}-\tau x\frac{\partial p}{\partial y}\right)$$
$$-\nu\left\{\frac{\partial}{\partial x}\frac{1}{M}\left(-M\frac{\partial w}{\partial x}+\tau y\frac{\partial u}{\partial x}-\tau x\frac{\partial u}{\partial y}+\kappa w-\tau v\right)\right.$$
$$\left.-\frac{\partial}{\partial y}\frac{1}{M}\left(M\frac{\partial w}{\partial y}-\tau y\frac{\partial v}{\partial x}+\tau x\frac{\partial v}{\partial y}-\tau u\right)\right\}. \tag{10a}$$

$$\frac{\partial u}{\partial t}+\left(u+\frac{\tau y}{M}w\right)\frac{\partial u}{\partial x}+\left(v-\frac{\tau x}{M}w\right)\frac{\partial u}{\partial y}+\frac{1}{M}w(\kappa w-\tau v)$$
$$=-\frac{1}{\rho}\frac{\partial p}{\partial x}-\frac{\nu}{M}\left\{M\frac{\partial}{\partial y}\left(\frac{\partial v}{\partial x}-\frac{\partial u}{\partial y}\right)\right.$$
$$+\left(-\tau y\frac{\partial}{\partial x}+\tau x\frac{\partial}{\partial y}\right)\frac{1}{M}\left(-M\frac{\partial w}{\partial x}+\tau y\frac{\partial u}{\partial x}\right.$$
$$\left.-\tau x\frac{\partial u}{\partial y}+\kappa w-\tau v\right)-\frac{\tau}{M}\left(M\frac{\partial w}{\partial y}-\tau y\frac{\partial v}{\partial x}\right.$$
$$\left.\left.+\tau x\frac{\partial v}{\partial y}-\tau u\right)\right\}. \tag{10b}$$

$$\frac{\partial v}{\partial t}+\left(u+\frac{\tau y}{M}w\right)\frac{\partial v}{\partial x}+\left(v-\frac{\tau x}{M}w\right)\frac{\partial v}{\partial y}+\frac{\tau}{M}wu$$
$$=-\frac{1}{\rho}\frac{\partial p}{\partial y}-\frac{\nu}{M}\left\{-M\frac{\partial}{\partial x}\left(\frac{\partial v}{\partial x}-\frac{\partial u}{\partial y}\right)\right.$$
$$+\left(\tau y\frac{\partial}{\partial x}-\tau x\frac{\partial}{\partial y}\right)\frac{1}{M}\left(M\frac{\partial w}{\partial y}-\tau y\frac{\partial v}{\partial x}+\tau x\frac{\partial v}{\partial y}-\tau u\right)$$
$$+\kappa\left(\frac{\partial v}{\partial x}-\frac{\partial u}{\partial y}\right)-\frac{\tau}{M}\left(-M\frac{\partial w}{\partial x}+\tau y\frac{\partial u}{\partial x}\right.$$
$$\left.\left.-\tau x\frac{\partial u}{\partial y}+\kappa w-\tau v\right)\right\}. \tag{10c}$$

where

$$M=1-\kappa x.$$

The assumption of a fully developed flow means that all s-derivatives are set to zero, except for the pressure derivative $\partial p/\partial s$, which is assumed to be constant.

The energy equation, assuming constant fluid properties and neglecting viscous dissipation, reads

$$\frac{\partial T}{\partial t}+\frac{w}{M}\frac{\partial T}{\partial s}+\left(u+\frac{\tau y}{M}w\right)\frac{\partial T}{\partial x}+\left(v-\frac{\tau x}{M}w\right)\frac{\partial T}{\partial y}$$
$$=\frac{\nu}{Pr}\frac{1}{M}\left\{\frac{\partial}{\partial s}\left(\frac{1}{M}\frac{\partial T}{\partial s}+\frac{\tau y}{M}\frac{\partial T}{\partial x}-\frac{\tau x}{M}\frac{\partial T}{\partial y}\right)\right.$$
$$+\frac{\partial}{\partial x}\left(\frac{\tau y}{M}\frac{\partial T}{\partial s}+\left(M+\frac{\tau^2y^2}{M}\right)\frac{\partial T}{\partial x}-\frac{\tau^2xy}{M}\frac{\partial T}{\partial y}\right)$$
$$\left.+\frac{\partial}{\partial y}\left(-\frac{\tau x}{M}\frac{\partial T}{\partial s}-\frac{\tau^2xy}{M}\frac{\partial T}{\partial x}+\left(M+\frac{\tau^2x^2}{M}\right)\frac{\partial T}{\partial y}\right)\right\}. \tag{11}$$

The present thermal boundary condition of constant axial wall heat flux, with uniform peripheral wall temperature, may be realized by assuming a temperature field of the form

$$T(s,x,y)=\gamma s+T_0(x,y), \tag{12}$$

with

$$T_0(x,y)=T_w=\text{constant at the wall.}$$

γ is then the constant axial temperature gradient. A dimensionless temperature may be defined by

$$\theta(x,y)=\frac{T_w-T_0(x,y)}{\gamma d_h}. \tag{13}$$

The local heat flux (directed inwards) normal to the duct wall is defined by

$$q_N=-k\frac{A_w}{A_{ws}}\nabla T\cdot\mathbf{N}, \tag{14}$$

where the temperature gradient is given by

$$\nabla T=\left(\frac{1}{M}\frac{\partial T}{\partial s}+\frac{\tau y}{M}\frac{\partial T}{\partial x}-\frac{\tau x}{M}\frac{\partial T}{\partial y}\right)\mathbf{t}+\frac{\partial T}{\partial x}\mathbf{n}+\frac{\partial T}{\partial y}\mathbf{b}, \tag{15}$$

and the inward-pointing unit normal

$$\left.\begin{aligned}\mathbf{N}&=(\tau y\mathbf{t}+M\mathbf{n})/\sqrt{\tau^2y^2+M^2},\quad \text{at } x=-a,\\ \mathbf{N}&=(-\tau x\mathbf{t}+M\mathbf{b})/\sqrt{\tau^2x^2+M^2},\quad \text{at } y=-b,\end{aligned}\right\} \tag{16}$$

and similarly with reversed sign at the walls $x=a$ and $y=b$, respectively. Note that for $\tau\neq 0$ the normal $\mathbf{N}$ will have a component in the direction of the tangent $\mathbf{t}$. In equation (14), A_w is the real (wetted) wall area of the duct, and A_{ws} the wall area for a straight duct with the same cross-section and length. A_w is obtained from

$$A_w=\iint_{x=\pm a}\mathrm{d}A_x+\iint_{y=\pm b}\mathrm{d}A_y, \tag{17}$$

where the area elements (and for completeness also the volume element) are given by

$$\left.\begin{aligned}\mathrm{d}A_x&=\sqrt{\tau^2y^2+M^2}\,\mathrm{d}s\,\mathrm{d}y,\quad \text{for } x=\text{const.}\\ \mathrm{d}A_y&=\sqrt{\tau^2x^2+M^2}\,\mathrm{d}s\,\mathrm{d}x,\quad \text{for } y=\text{const.}\\ \mathrm{d}A_s&=\mathrm{d}x\,\mathrm{d}y,\quad \text{for } s=\text{const.}\\ \mathrm{d}V&=M\,\mathrm{d}s\,\mathrm{d}x\,\mathrm{d}y\end{aligned}\right\} \tag{18}$$

By evaluating equation (17), one may conclude that for a duct with $\tau\neq 0$ the wall area will be greater than that of a straight (or toroidal) duct with the same

cross-section and length. This circumstance can cause difficulties in the actual manufacturing of helical rectangular ducts, since the material has to be stretched nonuniformly to obtain a correct cross-section. For a dimensionless torsion $\eta = \tau d_h = 1$ (the highest considered in this investigation), the wall area is about 4% larger than for a similar straight duct. An increased surface area will give an increased heat transport. Therefore, to allow a direct comparison with a straight duct, and also to avoid the evaluation of equation (17), the heat flux is defined according to equation (14). This means that, to obtain the heat transfer rate (in watts) for any duct, the heat flux q_N is to be multiplied by A_{ws}. The local heat transfer coefficient is defined by

$$h = \frac{q_N}{(T_w - T_b)}, \tag{19}$$

where T_b is the bulk mean temperature, which is given by

$$T_b = \frac{1}{\bar{w} 4ab} \iint_{\text{cross section}} Tw \, dA. \tag{20}$$

The local Nusselt number is defined by

$$Nu = \frac{h d_h}{k}. \tag{21}$$

The peripheral mean heat transfer coefficient h_m is defined by

$$h_m = \frac{q_{Nm}}{(T_w - T_b)}, \tag{22}$$

where q_{Nm} is the peripheral mean heat flux, which is obtained from

$$q_{Nm} = \frac{1}{4(a+b)} \int_{\text{periphery}} q_N \, dl. \tag{23}$$

By integrating the energy equation over a finite duct length, one may deduce the following alternative expression for the mean heat flux:

$$q_{Nm} = k\gamma PrRe/4. \tag{24}$$

For the mean Nusselt number one then obtains

$$Nu_m = \frac{h_m d_h}{k} = \frac{q_{Nm} d_h}{k(T_w - T_b)} = \frac{\gamma PrRe d_h}{4(T_w - T_b)}. \tag{25}$$

NUMERICAL PROCEDURE AND ESTIMATED ACCURACY

For constant fluid properties, the continuity and the Navier–Stokes equations may first be solved to obtain the velocity field. The energy equation is then solved for the temperature field. The procedure for obtaining the velocity field is described in more detail in refs. [4, 5]. In summary, the well-known finite volume method with a staggered grid is employed, see Patankar [17]. The hybrid difference scheme is employed, which formally is only first-order accurate. However, by using a sufficiently fine grid, in this case a uniform 41×41 grid, mostly central differences appear from the hybrid scheme, so that second-order accuracy is practically achieved. The velocity-pressure coupling is handled by using the SIMPLEC algorithm of Van Doormaal and Raithby [18]. Their recommended accelerated TDMA-solver was also found effective. The streamwise component of the pressure gradient is used as input to the computations, and the Reynolds number is then calculated from the converged solution.

The energy equation is solved according to a similar procedure. However, for Prandtl numbers greater than one, it was necessary to apply a higher order scheme for the convection terms to obtain an acceptable accuracy. This is so, since for high Prandtl numbers, the magnitude of the convection terms are enlarged compared to the diffusion terms. This means that an increased amount of upwind differencing will appear from the hybrid scheme, and accuracy is lost. The QUICK scheme by Leonard [19] was chosen, which in two dimensions should be second-order accurate. For Prandtl numbers less than one, the hybrid and the QUICK scheme gave identical results. Central differences were used for the diffusion terms and the source terms. The TDMA-solver [18], with a θ-value of 1.9, was used together with an ADI-technique, i.e. alternating sweeps in the x- and y-directions. An under-relaxation factor of 0.9 worked well for the lower Prandtl numbers. However, for highest Prandtl numbers, a factor as low as 0.35 proved necessary. No convergence problems were encountered, although many iterations (up to 100 000) were required for simultaneously high Dean ($De = Re\sqrt{\kappa d_h}$) and Prandtl numbers. The computations were carried out on a DEC 3000/400 AXP workstation.

Concerning the accuracy, we may at first conclude that the major part of the error is due to the discretization. The error due to an insufficient degree of convergence on a specific grid is negligible, since the convergence was in each case forced to the maximum capacity of the computer, using single precision arithmetics. This applies for both the velocity and the temperature fields. The convergence of the temperature field was also checked by comparing the mean heat fluxes obtained from the alternative equations (23) and (24). The difference was generally less than 0.01%, and at most 0.1% for the most severe cases. The discretization error was estimated by comparing the solutions obtained on three different uniform grids, 41×41, 61×61 and 81×81, respectively. Assuming second-order accuracy, h^2- or Richardson extrapolation (see ref. [5]) was also performed in a few cases to obtain fourth-order accuracy. For example, for $Pr = 10$ and $De = 510$ (the highest Dean number considered; at the four-vortex branch of the toroidal duct), the extrapolated mean Nusselt number, using the QUICK scheme and 61- and 81-grids, was determined to 20.5. A 6% higher value was obtained

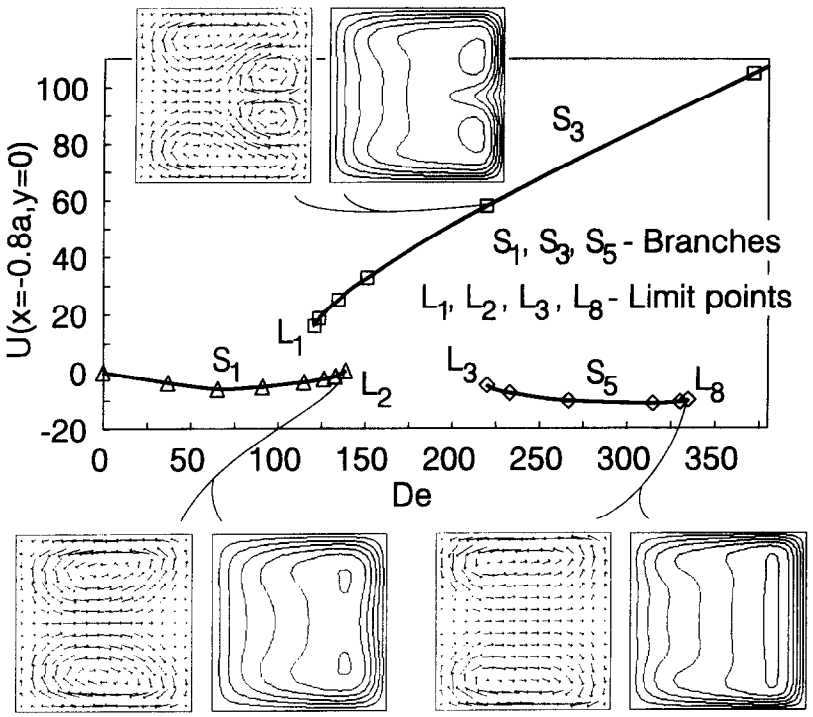

Fig. 2. State diagram for toroidal square duct with $\varepsilon = 0.2$. Secondary and axial flow at three states. Outer wall is to the right.

on a 41-grid, and a 2.6% higher on a 61-grid. Parenthetically, we note that the hybrid scheme produced a 40% too high value on a 41-grid for the same case. The above example is among the most severe ones considered, and for smaller Dean and Prandtl numbers the error is also smaller. For the highest Prandtl numbers of 100 and 500, the extrapolated values using 41- and 61-grids and 61- and 81-grids, respectively, did not always coincide. For example, at $De = 510$, the difference was 16% for $Pr = 500$ and 11% for $Pr = 100$. This is to be compared to a difference of 2.4% for $Pr = 30$ and only 0.2% for $Pr = 10$. For lower Dean numbers, the deviations are smaller. For example at L_8 ($De = 337$): 2.5% for $Pr = 500$ and 1.0% for $Pr = 100$. These results indicate that a 41-grid for high Prandtl and Dean numbers is insufficient to obtain second-order accuracy. In conclusion, a 41-grid is in most cases reasonable accurate, and this grid was mostly employed. For the severe cases, a 61-grid was adopted, but a few times also an 81-grid. The errors in the presented mean Nusselt numbers should at most be 3%, but are often less than 1.5%.

RESULTS AND DISCUSSION

Flow field

Figure 2 is a state diagram for a toroidal square duct with dimensionless curvature $\varepsilon = \kappa d_h = 0.2$. On the vertical axis is the dimensionless u-component of the secondary flow at a point close to the outer wall. Three solution branches were detected, denoted by S_1, S_3 and S_5. The end points of the branches are called limit points, and they are denoted by L_1, L_2, L_3 and L_8, respectively, following the notations employed by Winters [10]. The precise locations of the limit points have been determined in ref. [5], using h^2-extrapolation. The present solution method is transient, as opposed to direct, which means that only stable solution branches can be detected. S_1 and S_5 are unconditionally stable branches characterized by the secondary flow having two symmetric counter-rotating vortices. This is seen in the vector plots in Fig. 2, where contours of the axial flow are also given, and we note that the maximum of the axial flow is shifted towards the outer wall. The S_3 branch is unstable for asymmetric perturbations, and could only be detected by imposing symmetry about the x-axis. Solutions of the S_3 branch have a pair of extra counter-rotating vortices at the outer wall, and where these occur the axial flow has a depression. Converged solutions of the S_3 branch were obtained up to a Dean number of about 550, no precise upper limit was determined.

Figure 3 shows the extent of the S_1 and S_5 branches for helical square ducts with $\varepsilon = 0.2$ and increasing torsion η. S_3 could not be detected for a finite torsion. For ducts with small torsion, both the flow field and the extent of the detected branches are similar to the conditions for a toroidal duct with the same dimensionless curvature ε. The lower vortex of the secondary flow is enlarged at the expense of the upper vortex, and the axial flow only shows a very slight asymmetry. For higher torsion, the S_5 branch could not be detected, and the extent of the S_1 branch at first decreases, and for even higher torsion it then increases

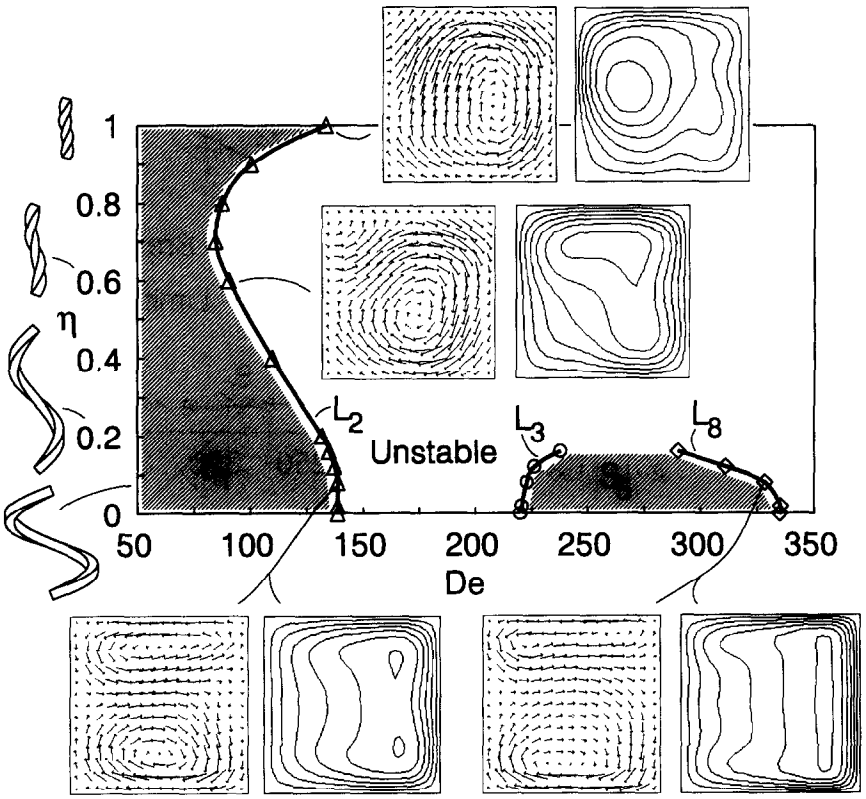

Fig. 3. Extent of S_1 and S_5 branches for helical square ducts with $\varepsilon = 0.2$. Secondary and axial flow at four states. Outer wall is to the right.

to higher Dean numbers again. For high enough torsion, the secondary flow approaches a one-vortex structure, and the maximum of the axial flow is shifted towards the inner wall.

For certain Dean numbers, no unconditionally stable, fully developed flow solutions are obtained, as for example between the S_1 and S_5 branches, and above S_5. If one performs unsteady, fully developed computations without assuming symmetry for Dean numbers between L_2 and L_3, the flow is found to oscillate regularly between a two-vortex and a four-vortex structure. For a helical square duct, this is shown in Bolinder and Sundén [6]. An analogous behaviour is reported by Sankar *et al.* [21] and Bara *et al.* [22], in their steady and parabolic computations of developing flow in a toroidal square duct; for Dean numbers between L_2 and L_3, spatial oscillations develop, alternating between a two-vortex and a four-vortex structure. To reveal a more exact nature of the oscillations, it might be necessary to perform unsteady and fully elliptic computations of developing flow. In the experiments in ref. [6], a steady two-vortex flow was normally obtained for Dean numbers between L_2 and L_3, where the fully developed numerical computations predicted an oscillating flow. Only by disturbing the flow at the inlet of the duct, a four-vortex flow could occasionally be realized. For Dean numbers above L_8, transition phenomena eventually appear. According to the unsteady computations and the experiments in ref. [6], extra vortices emerge spontaneously and irregularly from the outer wall, with an increasing frequency for increasing Dean numbers above L_8. Mori *et al.* [8] detected transition at $De = 850$ in their experiments, and for $De > 2500$ the flow was fully turbulent. Some of the axial flow profiles in the paper by Eason *et al.* [14] show a depression at the outer wall, which indicates occurrences of extra vortices.

Temperature field

Figures 4 and 5 show contours of the dimensionless temperature θ at the same states as in Figs. 2 and 3. For ducts of small and moderate pitch, the appearance of the temperature field depends highly on the Prandtl number. For $Pr = 0.01$, characteristic of liquid metals, the diffusion terms dominate in the energy equation, and the secondary flow influences the temperature field only to a very slight extent. According to Fig. 5(a), for ducts of small torsion, the position of maximum temperature (or minimum, if the fluid is heated) is moved somewhat towards the outer wall, while for a high torsion the maximum is moved instead towards the inner wall, but the overall distortion of the temperature field is small.

For a Prandtl number of 0.71, characteristic of gases, the temperature profiles are similar to the axial flow profiles, see Figs. 4 and 5(a). Thus, for a small torsion, the position of maximum temperature is

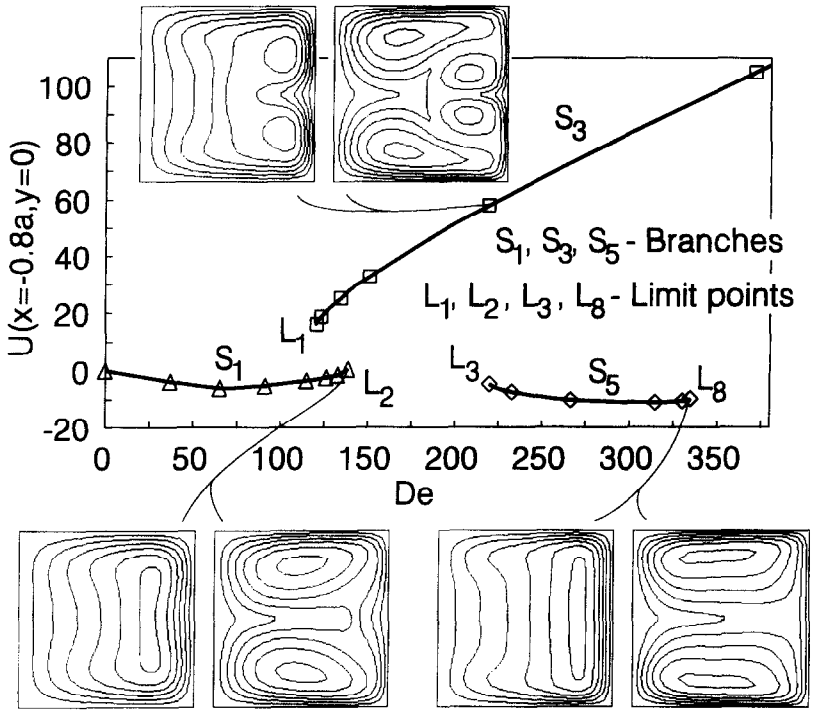

Fig. 4. Diagram as in Fig. 2. θ-contours for $Pr = 0.71$ (left) and $Pr = 10$ (right).

shifted towards the outer wall, and the torsion only causes a slight asymmetry. For Prandtl numbers greater than one, characteristic of various liquids, the convection terms in the energy equation become more important, and the θ-contours resemble streamlines of the secondary flow, see Figs. 4 and 5(b).

While the Prandtl number greatly affects the shape of the temperature field for ducts of small torsion, the effect diminishes for increasing torsion. For example, for $\eta = 1$ in Fig. 5(a, b), the θ-plots are all quite similar, even though the Prandtl number varies between 0.01 and 100. The effect of torsion on the temperature field seems to increase slightly for increasing Prandtl numbers; the θ-plots in Fig. 5(a, b) become more asymmetric as the Prandtl number increases.

In Fig. 6 three-dimensional-plots of the temperature field for a toroidal square duct at the upper limit of the S_5 branch for Prandtl numbers between 0.71 and 100 are shown. For increasing Pr, the effect of diffusion diminishes, and cold fluid (or hot, in the case of heating) at the inner wall is carried by the secondary flow farther towards the outer wall without being diffused. Note also the quite similar profiles for $Pr = 10$ and 100, which indicates an independence of the Prandtl number for high enough Pr.

In Fig. 7 three-dimensional-plots of θ for solutions of the S_3 branch, i.e. the branch characterized by the secondary flow having two extra vortices at the outer wall are shown, see Fig. 2. For $Pr = 0.71$, the θ-profile resembles the axial flow profile as usual. For $Pr > 1$, two extra 'bumps' in the θ-profile appear at the location of the extra vortices. The base level of these extra bumps is lowered for increasing Pr, and it is likely that for high enough Pr a limit is reached. The computations for $Pr = 500$ indicated a flattening of the extra bumps, and for even higher Pr the extra bumps may totally disappear. However, the numerical uncertainties for high Prandtl numbers prevent a definite conclusion in this matter.

Mean Nusselt numbers

The results above for the temperature field showed that the effect of a small or moderate pitch is minor. Therefore, the Nusselt number results for toroidal square ducts will first be discussed quite extensively, and then the validity of the results for helical ducts is pointed out. Figure 8 shows the Nusselt number ratio $Nu_m/(Nu_m)_s$ for a toroidal square duct and for $Pr = 0.71$. The index s refers to a straight duct, for which $Nu_m = 3.608$ for the $H1$ boundary condition, see Shah and London [23]. Note that the S_3 branch (the one with the extra vortices) has slightly higher Nusselt numbers than the S_5 branch. This can be explained by the additional stirring caused by the extra vortices. In Fig. 8 a few results found in the literature are also shown. The agreement is generally good, despite the consideration of the different curvatures and thermal boundary conditions. That is, the curvature effect seems to be well captured by the Dean number alone, and the particular thermal boundary condition applied seems less important.

To obtain a quantitative check on the effect of curvature, the Nusselt number ratio was computed for two additional ducts with $\varepsilon = 0.04$ and 0.47, respectively. The Nusselt numbers were compared at the Dean numbers 128, 220 and 310, of the S_1, S_3 and S_5

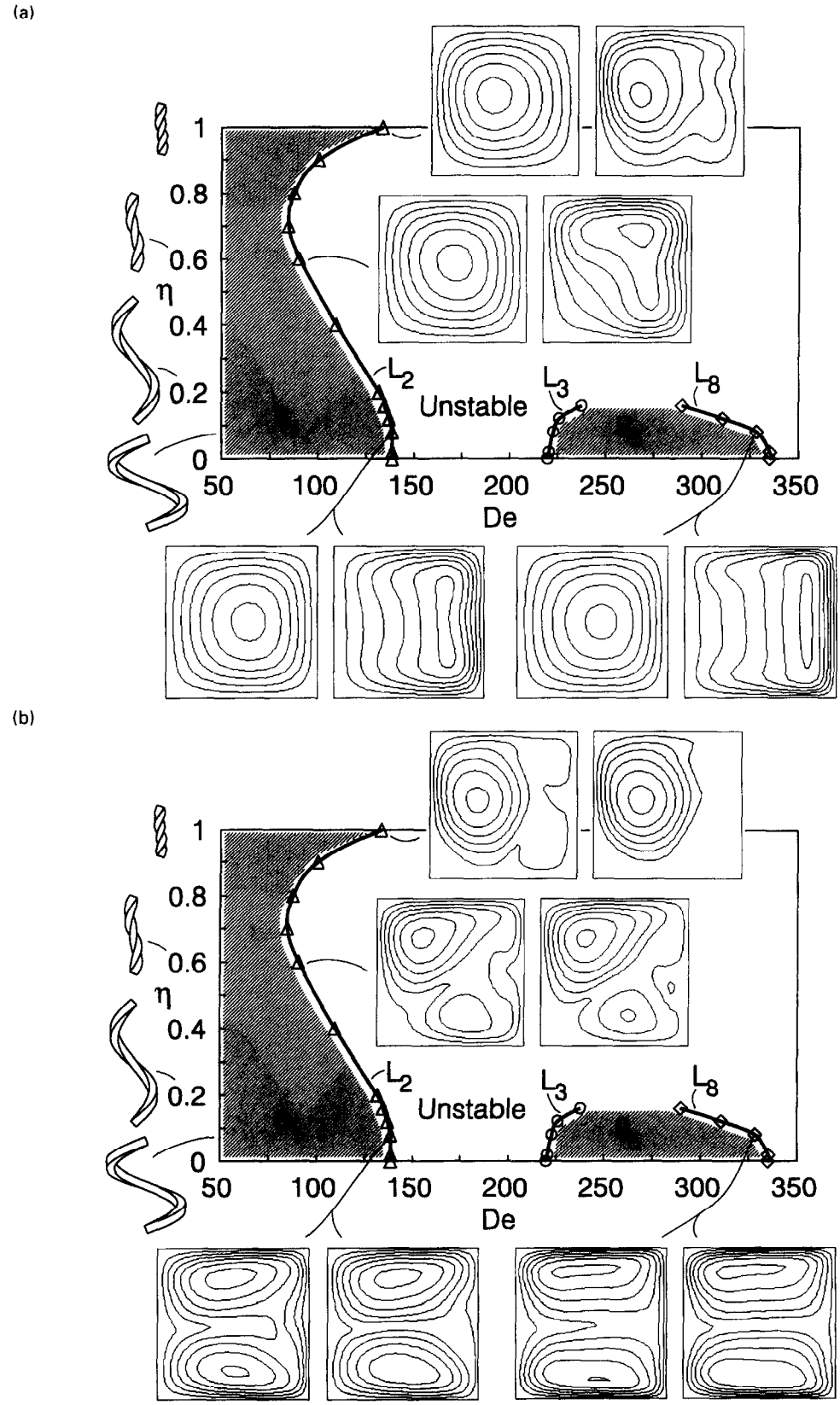

Fig. 5. (a) Diagram as in Fig. 3. θ-contours for $Pr = 0.01$ (left) and $Pr = 0.71$ (right). (b) Diagram as in Fig. 3. θ-contours for $Pr = 10$ (left) and $Pr = 100$ (right).

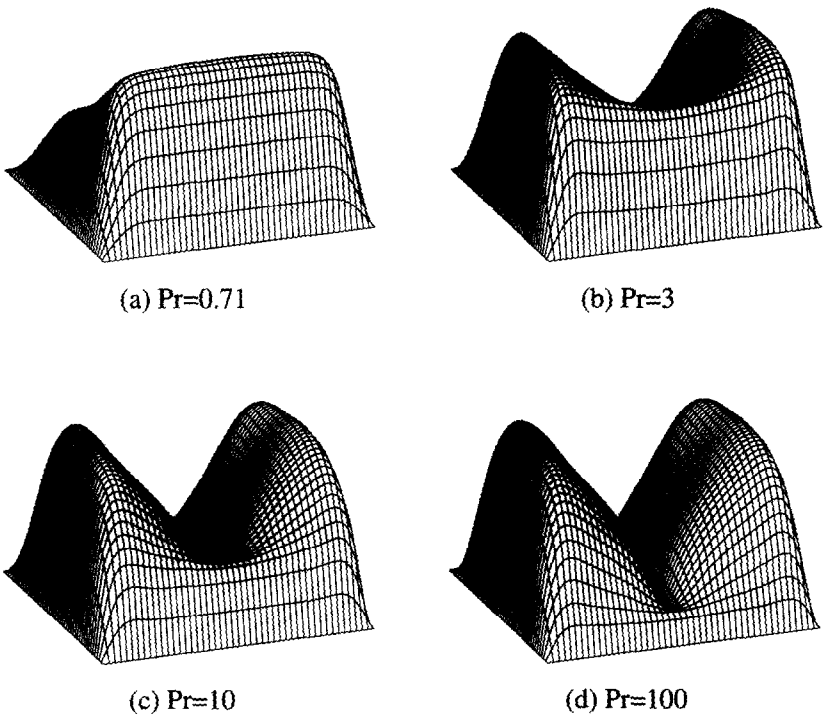

Fig. 6. Temperature profiles for toroidal square duct with $\varepsilon = 0.2$. S_5 branch at $De = 335$. Viewed from outer wall.

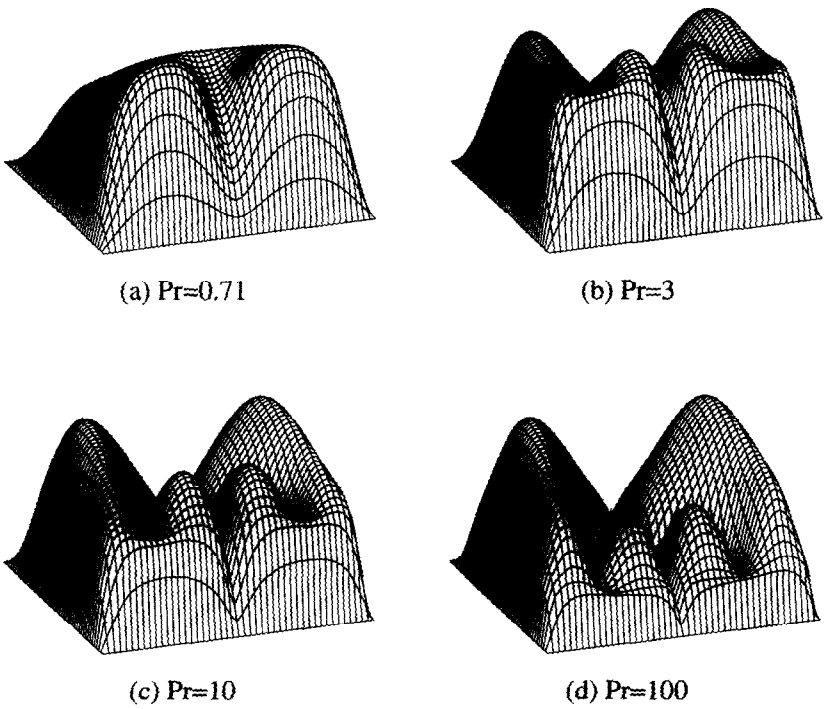

Fig. 7. Temperature profiles for toroidal square duct with $\varepsilon = 0.2$ and S_3 branch at $De = 220$. Viewed from outer wall.

branches, respectively. Prandtl numbers between 0.01 and 100 were considered. Compared to the duct with $\varepsilon = 0.2$, the deviations in the Nusselt number ratio were generally less than 2%, except for $\varepsilon = 0.04$ at $De = 128$ and $Pr \geqslant 10$, under which conditions the Nusselt number ratio was up to 4% higher than for $\varepsilon = 0.2$ under the same conditions. Compared to the results for the friction factor ratio $fRe/(fRe)_s$ given in ref. [5], the Nusselt number ratio is somewhat less sensitive to variations in the curvature.

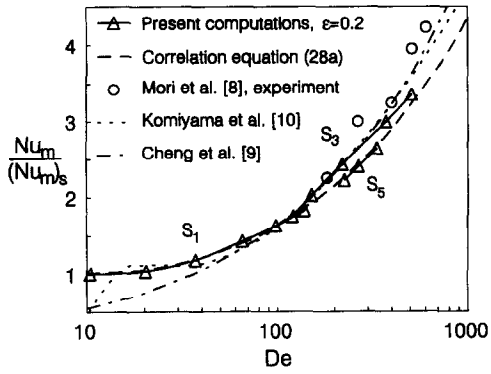

Fig. 8. Comparison of a few results for toroidal square ducts, $Pr = 0.71$.

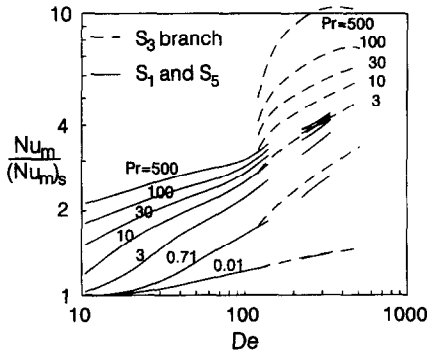

Fig. 9. Computed mean Nusselt numbers for toroidal square duct with $\varepsilon = 0.2$ and with Prandtl number as parameter.

Figure 9 shows how the Prandtl number affects the Nusselt number ratio for a toroidal square duct. In general, the Nusselt number is increased for increasing Pr. However, the Nusselt numbers of the S_5 branch reach an upper limit for the range of Prandtl numbers considered. The highest values of the S_5 branch are obtained for $Pr = 100$. For $Pr = 500$, the Nusselt numbers fall somewhat below those for $Pr = 100$, and the slope of the curve is not so steep. Note that, for high Prandtl numbers, the Nusselt number ratio is significantly greater than one for a Dean number as low as 10. Note also that the gap between the S_3 and S_5 branches increases with increasing Pr. For $Pr = 0.01$, S_3 and S_5 fall almost on top of each other, and for $Pr = 500$, the Nusselt numbers of the S_3 branch are more than twice those of the S_5 branch. Thus, if a flow field of the S_3 branch could be realized in an application with a high Prandtl number fluid, a significant improvement of the heat transfer rate would result. The potential for obtaining extra vortices will be further discussed in the concluding section.

For curved ducts of both circular and rectangular cross-sections, it is often found that the friction factor ratio and the Nusselt number ratio are proportional to the square root of the Dean number in the upper laminar regime. This is the case, for example, in the Nusselt number correlation given by Cheng *et al.* [9], and also in the friction factor correlation given in ref. [5], which reads

$$\frac{fRe}{(fRe)_s} = (1 + 0.288De + 8.8 \cdot 10^{-8} De^4)^{-0.3} + 0.107\sqrt{De} \quad De < 1500 \quad \varepsilon < 0.4, \frac{\eta}{\varepsilon} \leqslant 1. \quad (26)$$

Equation (26) gives correct values in both the limits of high and low Dean numbers, and for $\varepsilon = 0.2$ it deviates by less than 2% from the computed values of the two-vortex branches. However, for $De < 6$ it is recommended to use $fRe/(fRe)_s = 1$. For the present computations, the slope of the S_5 branches for the various Prandtl numbers was used as an indication of the asymptotic Dean number dependence. For $Pr \geqslant 0.71$, a Dean number exponent of 0.4–0.45 was obtained, with a tendency of decreasing exponent for the highest Pr. These values are quite close to the commonly assumed value of 0.5. Based on the computed Nusselt numbers of the S_5 branch, the following asymptotic correlations are proposed:

$$Nu_m/(Nu_m)_s = 0.7De^{0.12} \quad 0.005 \leqslant Pr \leqslant 0.02 \quad De > 25 \quad (27a)$$

$$Nu_m/(Nu_m)_s = 0.213Pr^{0.27}De^{0.45} \quad 0.71 \leqslant Pr \leqslant 2 \quad De > 150 \quad (27b)$$

$$Nu_m/(Nu_m)_s = 0.278Pr^{0.09}De^{0.43} \quad 2 < Pr \leqslant 15 \quad De > 100 \quad (27c)$$

$$Nu_m/(Nu_m)_s = 0.38Pr^{0.03}De^{0.4} \quad 10 \leqslant Pr < 500 \quad De > 150. \quad (27d)$$

For all correlations it is assumed that

$$De < 1500 \quad \varepsilon < 0.5 \quad \eta/\varepsilon \leqslant 1.$$

The upper Dean number limit is determined by the requirement that the flow is to be laminar and of two-vortex type, i.e. no extra vortices are allowed. The upper limit is arbitrary set to 1500, and this value may be higher or lower, depending on the actual flow conditions. For example, it is likely that induced disturbances in the flow promote the formation of extra vortices, and thus reduce the range of validity of equation (27a–d), compared with the discussion about the flow field above. The lower Dean number limit is indicated for each equation. For Dean numbers between the S_1 and S_5 branches (i.e. between L_2 and L_3), it is assumed that the Nusselt number can be obtained by an interpolation between the branches. Equation (27a) is valid for the S_3 branch as well, and it deviates by less than 1% from the computed values. Equation (27b) deviates by less than 3% and equation (27c, d) by less than 2.3% from the computed values. For Prandtl numbers between 0.71 and 2 it was possible to extend the range of validity of the asymptotic correlation by adding a term similar to the one in

equation (26). Thus, the following correlations are proposed:

$$Nu_m/(Nu_m)_s = (1+0.122De)^{-0.95} + 0.213Pr^{0.27}De^{0.45} \quad Pr = 0.71 \quad (28a)$$

$$Nu_m/(Nu_m)_s = (1+0.46De)^{-0.6} + 0.213Pr^{0.27}De^{0.45} \quad Pr = 1 \quad (28b)$$

$$Nu_m/(Nu_m)_s = (1+0.94De)^{-0.55} + 0.213Pr^{0.27}De^{0.45} \quad Pr = 1.5 \quad (28c)$$

$$Nu_m/(Nu_m)_s = (1+1.8De)^{-0.5} + 0.213Pr^{0.27}De^{0.45} \quad Pr = 2. \quad (28d)$$

For all correlations it is assumed that

$$15 < De < 1500 \quad \varepsilon < 0.5 \quad \text{and} \quad \eta/\varepsilon \leqslant 1.$$

Even though the correlations are asymptotically correct for low Dean numbers, less error is often obtained by using $Nu_m/(Nu_m)_s = 1$ for $De < 15$. Equations (28a–d) deviate by less than 2.1% from the computed values of the S_1 and S_5 branches (for $De > 15$). Equation (28a) is plotted in Fig. 8.

An effect of curvature is to increase the mean Nusselt number. This increase, however, is accompanied by increased frictional losses. Following Kalb and Seader [24], a measure of the efficiency E of using curved ducts instead of straight ones is given by the Nusselt number ratio divided by the friction factor ratio, i.e.

$$E = \frac{Nu_m/(Nu_m)_s}{fRe/(fRe)_s}. \quad (29)$$

An efficiency greater than one indicates a better performance of curved ducts than of straight ones. For solutions of the S_5 branch, E is about 0.7 for $Pr = 0.01$, about 1.3 for $Pr = 0.71$ and about 2.0 for $Pr = 10$. These values are similar to those obtained by Kalb and Seader [24], for ducts with a circular cross-section.

The effect of torsion on the mean Nusselt number is indicated in Fig. 10. Note that the Reynolds number on the horizontal axis allows for a comparison with the straight twisted duct, for which the Dean number is not defined. Only Nusselt numbers of the S_1 branch are plotted in Fig. 10. S_5 could only be detected for $\eta \leqslant 0.16$, and for such a low torsion the Nusselt numbers of the S_5 branch are almost identical to the values for a toroidal duct with the same dimensionless curvature ε. Also for the S_1 branch, the Nusselt number is hardly affected by a small torsion, even though a decreased value is obtained for smaller Reynolds numbers, and especially if the Prandtl number is high, see Fig. 10. For Reynolds numbers close to the upper limit L_2, a slight increase in the Nusselt number is obtained for ducts of moderate torsion. For ducts of large torsion, the Nusselt number approaches the value for a straight twisted duct, which is slightly less than that for a straight duct. In conclusion, at least for $\eta/\varepsilon \leqslant 1$, equations (27) and (28) for the Nusselt number ratio are applicable. Note that for a straight twisted duct, the Nusselt number is almost insensitive to variations in Prandtl and Reynolds numbers. This behaviour is in accordance with the results of Masliyah and Nandakumar [15], who applied the T boundary condition. Finally, in comparison with the results in ref. [5], we note that the friction factor is less affected by torsion than the Nusselt number.

Local Nusselt numbers

In Fig. 11 the local Nusselt number variation along the periphery for a toroidal square duct is shown. The conditions at the upper limit of the S_5 branch [Fig. 11(a)], and at a position of the S_3 branch [Fig. 11(b)] are given. Due to symmetry, only the variation along the upper half of the cross-section is indicated. The Nusselt number variation increases with increasing Pr, and higher values are generally obtained towards the outer wall. For the S_5 branch, with a two-vortex secondary flow, the local Nusselt number shows a flat profile along the outer wall, and for increasing Pr, an upper limit is quickly reached, see Fig. 11(a). In fact, the mean Nusselt number along the outer wall is almost the same for $Pr = 0.71$ and 100. For the S_3 branch, with a four-vortex secondary flow, the mean Nusselt number along the outer wall instead increases continuously with increasing Pr, see Fig. 11(b), and the local Nusselt number varies strongly, with minima at the corners and at the symmetry line $y = 0$. These different behaviours 'explain' why the mean Nusselt numbers of S_5 reach an upper limit for the range of Prandtl numbers considered, but not the Nusselt numbers of S_3. Due to the uniform wall temperature, the local Nusselt number drops to zero at the corners. In fact, precisely at the corners, the Nusselt number is not defined, since the normal in equation (16) is not defined. We could define the normal, at a corner for example, as the normalized vector sum of the expressions given in equation (16). Then, the local Nusselt number would be nonzero at the corners, thus yielding a discontinuous variation along the periphery.

For helical ducts with a finite pitch, the local Nusselt number is asymmetric about $y = 0$. According to Fig. 12, which shows the local Nusselt number variation for a helical square duct with a relatively large pitch, the degree of asymmetry is quite moderate, even though an increased asymmetry can be observed for increasing Pr. We also note that the local Nusselt number can be estimated from the θ-contours provided in Fig. 12.

Figure 13 shows the local Nusselt number variation for a helical duct with a large torsion compared to the curvature. The highest Nusselt numbers are now obtained along the inner wall. Note that, for a low Prandtl number of 0.01 [Fig. 13(a)], the Nusselt number is discontinuous at the corners; a positive Nu is obtained when approaching the corner from one wall,

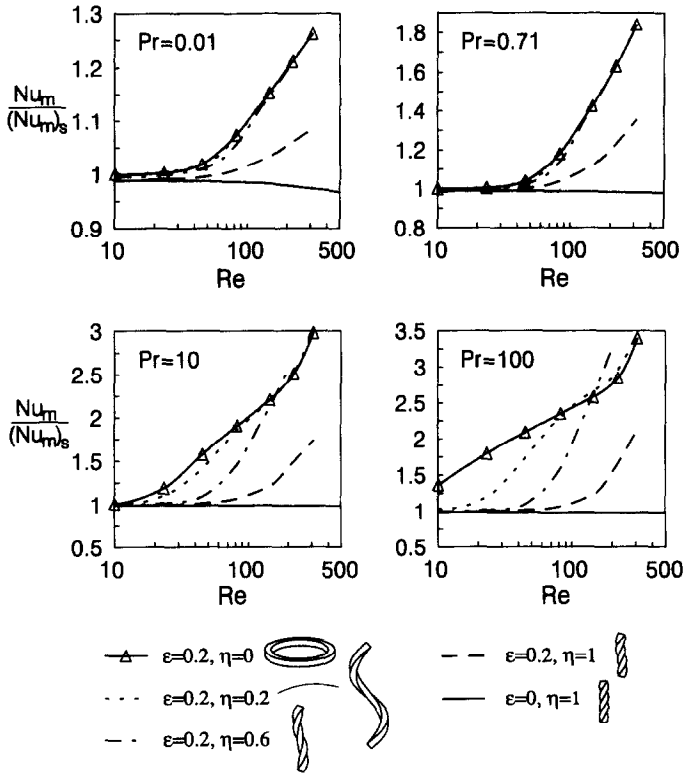

Fig. 10. Computed mean Nusselt numbers for helical square ducts.

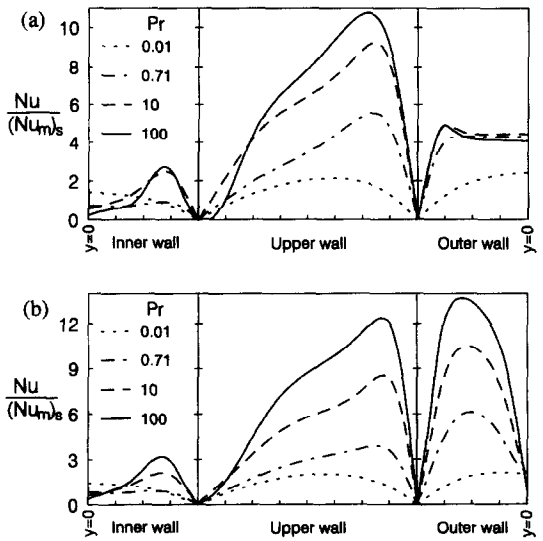

Fig. 11. Local Nusselt number variation along periphery for toroidal square duct with $\varepsilon = 0.2$. (a) S_5 branch at $De = 335$. (b) S_3 branch at $De = 220$.

and a negative Nu is obtained when approaching from the other wall. This is explained by the fact that for $\tau \neq 0$, the normal to the duct wall has alternating positive and negative components in the axial direction at either side of the corners, see equation (16). Thus, when the torsion is large and the temperature gradients in the cross-section are small in comparison to the axial temperature gradient γ, which is the case for small Prandtl numbers, then the heat flux in the axial direction influences the local Nusselt number significantly, and a situation as in Fig. 13(a) is obtained. Actually, for all ducts with $\tau \neq 0$, the Nusselt number is discontinuous at the corners, but the discontinuity is normally very small. For example, if the Prandtl number is increased to 0.71, as in Fig. 13(b), the discontinuity cannot be distinguished. For the extreme cases with high torsion and low Prandtl numbers, the local Nusselt number cannot be estimated from the θ-contours. It would be possible to avoid the discontinuous Nusselt numbers by using a different heat flux in the definition of the heat transfer coefficient, equation (19). Instead of using the heat flux normal to the duct wall, q_N, we could use the heat flux in the directions obtained by forcing τ to zero in equation (16), i.e. in the $\mathbf{n}$-direction at $x = -a$, and in the $\mathbf{b}$-direction at $y = -b$ (and with reversed sign at $x = a$ and $y = b$, respectively).

CONCLUDING REMARKS

Fully developed laminar forced convective heat transfer in helical square ducts has been investigated numerically using the finite-volume method. Stable flow solutions, belonging to different solution branches, are only obtained for limited Dean number intervals. For ducts of small pitch or torsion, the flow and heat transfer characteristics are similar to those of a toroidal duct with the same dimensionless curvature ε.

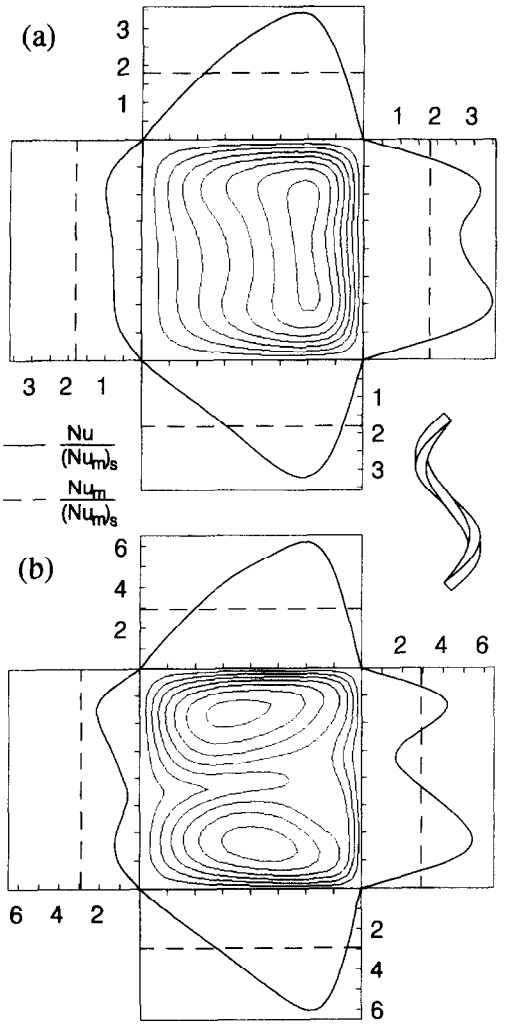

Fig. 12. Local Nusselt number variation along periphery for helical square duct with $\varepsilon = \eta = 0.2$, $De = 132$. Outer wall is to the right. (a) $Pr = 0.71$, (b) $Pr = 10$.

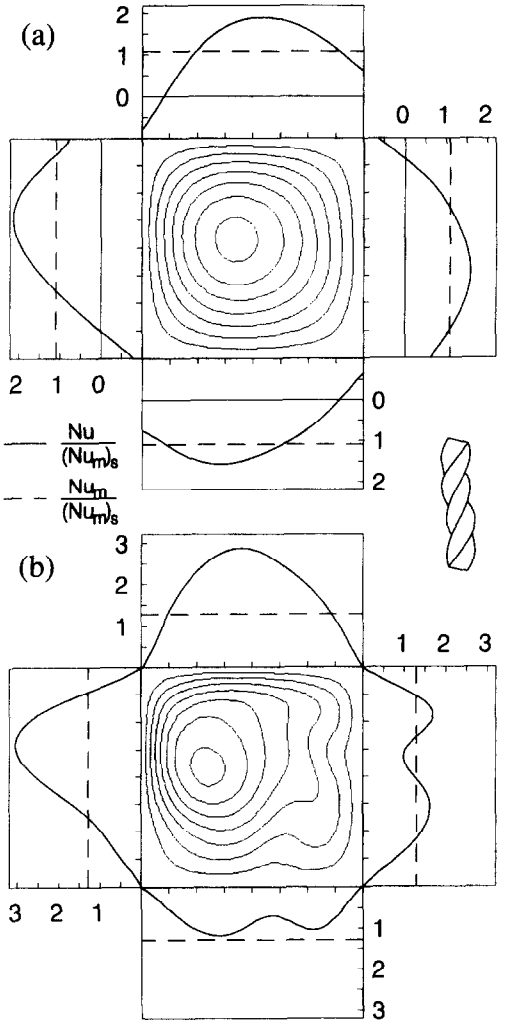

Fig. 13. Local Nusselt number variation along periphery for helical square duct with $\varepsilon = 0.2$ and $\eta = 1$, $De = 135$. Outer wall is to the right. (a) $Pr = 0.01$. (b) $Pr = 0.71$.

The temperature field is highly affected by the Prandtl number. The mean Nusselt number normally increases with increasing Pr, but for the S_5 branch an upper limit is reached for Pr about 100. The gap in the mean Nusselt number between the two-vortex S_5 branch and the four-vortex S_3 branch increases with increasing Pr, and for Pr equal to 500, the mean Nusselt number of the S_3 branch is twice that of the S_5 branch. Thus, in an application with a high Prandtl number fluid, it might be favourable to obtain a four-vortex flow, if a high heat transfer rate is desired. Bara *et al.* [22], in their experiments on developing laminar flow in a toroidal square duct, obtained a four-vortex flow by disturbing the flow at the outer wall at the inlet using a symmetrically positioned small pin. In the experiments on flow in a helical square duct with a finite pitch by Bolinder and Sundén [6], a similar arrangement with a small pin however, did, not prove effective in obtaining a four-vortex flow. More extensive disturbances seemed to be necessary. A stable four-vortex flow is probably more difficult to obtain in a helical duct with a finite pitch than in a toroidal duct, due to the inherent asymmetry of a helical duct. Another way to obtain an increased heat transfer rate would be to utilize transitional flow, which is characterized by unsteady extra vortices emerging from the outer wall. According to ref. [6], for a curved square duct, transition phenomena often seem to appear at lower Reynolds numbers than for a straight duct.

REFERENCES

1. R. K. Shah and S. D. Joshi, Convective heat transfer in curved ducts. In *Handbook of Single-Phase Convective Heat Transfer* (Edited by S. Kakac, R. K. Shah and W. Aung), Wiley, New York (1987).
2. S. A. Berger, L. Talbot and L.-S. Yao, Flow in curved pipes, *Ann. Rev. Fluid Mech.* **15**, 461–512 (1983).
3. K. Nandakumar and J. H. Masliyah, Swirling flow and heat transfer in coiled and twisted pipes. In *Advances in Transport Processes* (Edited by A. S. Mujumdar and R.

A. Mashelkar), Vol. IV, pp. 49–112, Wiley, New York (1986).
4. C. J. Bolinder, Numerical visualization of the flow in a helical duct of rectangular cross-section, *Expl. Numer. Flow Visualization ASME* **172,** 329–338 (1993).
5. C. J. Bolinder, The effect of torsion on the bifurcation structure of laminar flow in a helical square duct, *ASME J. Fluids Engng* **117,** 242–248 (1995).
6. C. J. Bolinder and B. Sundén, Flow visualization and LDV measurements of laminar flow in a helical square duct with a finite pitch, *Exp. Thermal Fluid Sci.* **11,** 348–363 (1995).
7. K. C. Cheng and M. Akiyama, Laminar forced convection heat transfer in curved rectangular channels, *Int. J. Heat Mass Transfer* **13,** 471–490 (1970).
8. Y. Mori, Y. Uchida and T. Ukon, Forced convective heat transfer in a curved channel with a square cross-section, *Int. J. Heat Mass Transfer* **14,** 1787–1805 (1971).
9. K. C. Cheng, R. C. Lin and J. W. Ou, Graetz problem in curved square channels, *ASME J. Heat Transfer* **97,** 244–248 (1975).
10. Y. Komiyama, F. Mikami, K. Okui and T. Hori, Laminar forced convection heat transfer in curved channels of rectangular cross-section, *Heat Transfer-Jpn. Res.* **13,** 68–91 (1984).
11. G. J. Hwang and C.-H. Chao, Forced laminar convection in a curved isothermal square duct, *ASME J. Heat Transfer* **113,** 48–55 (1991).
12. G. Yang, Z. F. Dong and M. A. Ebadian, The effect of torsion on convective heat transfer in a helicoidal pipe, *ASME J. Heat Transfer* **115,** 796–800 (1993).
13. S. Liu and J. H. Masliyah, Developing convective heat transfer in helical pipes with finite pitch, *Int. J. Heat Fluid Flow* **15,** 66–74 (1994).
14. R. M. Eason, Y. Bayazitoglu and A. Meade, Enhancement of heat transfer in square helical ducts, *Int. J. Heat Mass Transfer* **37,** 2077–2087 (1994).
15. J. H. Masliyah and K. Nandakumar, Steady laminar flow through twisted pipes: heat transfer in square tubes, *ASME J. Heat Transfer* **103,** 791–796 (1981).
16. K. Nandakumar and J. H. Masliyah, Steady laminar flow through twisted pipes: fluid flow and heat transfer in rectangular tubes, *Chem. Engng Commun.* **21,** 151–173 (1983).
17. S. V. Patankar, *Numerical Heat Transfer and Fluid Flow*. McGraw-Hill, New York (1980).
18. J. P. Van Doormaal and G. D. Raithby, Enhancements of the SIMPLE method for predicting incompressible fluid flows, *Numer. Heat Transfer* **7,** 147–163 (1984).
19. B. P. Leonard, A stable and accurate convective modelling procedure based on quadratic upstream interpolation, *Comput. Meth. Appl. Mech. Engng* **19,** 59–98 (1979).
20. K. H. Winters, A bifurcation study of laminar flow in a curved tube of rectangular cross-section, *J. Fluid Mech.* **180,** 343–369 (1987).
21. S. R. Sankar, K. Nandakumar and J. H. Masliyah, Oscillatory flows in coiled square ducts, *Phys. Fluids* **31,** 1348–1359 (1988).
22. B. Bara, K. Nandakumar and J. H. Masliyah, An experimental and numerical study of the Dean problem: flow development towards two-dimensional multiple solutions, *J. Fluid Mech.* **244,** 339–376 (1992).
23. R. K. Shah and A. L. London, *Advances in Heat Transfer*, Suppl. 1, *Laminar Flow Forced Convection in Ducts*, p. 200. Academic Press, New York (1978).
24. C. E. Kalb and J. D. Seader, Heat and mass transfer phenomena for viscous flow in curved circular tubes, *Int. J. Heat Mass Transfer* **15,** 801–817 (1972).